

Radial and spiral stream formation in *Proteus mirabilis* colonies

Chuan Xue^{1,*}, Elena O. Budrene², Hans G. Othmer³

¹ Mathematical Biosciences Institute, the Ohio State University, Columbus, OH, USA

² Department of Mathematics, Massachusetts Institute of Technology, Cambridge, MA, USA

³ School of Mathematics and Digital Technology Center, University of Minnesota, Minneapolis, MN, USA

* E-mail: cxue@mbi.osu.edu

Abstract

The enteric bacterium *Proteus mirabilis*, which is a pathogen that forms biofilms *in vivo*, can swarm over hard surfaces and form concentric ring patterns in colonies. Colony formation involves two distinct cell types: swarmer cells that dominate near the surface and the leading edge, and swimmer cells that prefer a less viscous medium, but the mechanisms underlying pattern formation are not understood. New experimental investigations reported here show that swimmer cells in the center of the colony stream inward toward the inoculation site and in the process form many complex patterns, including radial and spiral streams, in addition to concentric rings. These new observations suggest that swimmers are motile and that indirect interactions between them are essential in the pattern formation. To explain these observations we develop a hybrid cell-based model that incorporates a chemotactic response of swimmers to a chemical they produce. The model predicts that formation of radial streams can be explained as the modulation of the local attractant concentration by the cells, and that the chirality of the spiral streams can be predicted by incorporating a swimming bias of the cells near the surface of the substrate. The spatial patterns generated from the model are in qualitative agreement with the experimental observations.

Introduction

A variety of spatial patterns in growing bacterial colonies are found in nature and in the lab [1–10]. When grown on semi-solid agar with succinate or other TCA cycle intermediates, *Escherichia coli* cells divide, move and selforganize into patterns ranging from outward-moving rings of high cell density to chevron patterns, depending on the initial concentration of the nutrient [1, 2]. When grown or just placed in static liquids, cells quickly reorganize into networks of high cell density comprised of bands and/or aggregates, after exposure to succinate and other compounds. Chemotactic strains of *Salmonella typhimurium*, a closely-related species, can also form concentric rings and other complex patterns in similar conditions [3, 4]. It has been shown that pattern formation in *E. coli* and *S. typhimurium* is caused by chemotactic interactions between the cells and a self-produced attractant [1–3]. The gram-positive bacterium *Bacillus subtilis* forms patterns ranging from highly branched fractal-like patterns to compact forms, depending on the agar and nutrient concentrations [5, 6]. In all these systems proliferation, metabolism and movement of individual cells, as well as direct and indirect interactions between cells, are involved in the patterning process, but how they influence each other and what balances between them lead to the different types of patterns can best be explored with

a mathematical model. Understanding these balances would advance our understanding of the formation of more complex biofilms and other multicellular assemblies [11].

Proteus mirabilis is an enteric gram-negative bacterium that causes urinary tract infections, kidney stones and other diseases [12–15]. *P. mirabilis* is also known for spectacular patterns of concentric rings or spirals that form in *Proteus* colonies when grown on hard agar. Pattern formation by *Proteus* was described over 100 years ago [16], and the nature of these patterns has since been discussed in many publications.

P. mirabilis cells grown in liquid medium are vegetative swimmer cells which are 1-2 μm long, have 1-10 flagella and move using a “run-and-tumble strategy”, similar to that used by *E. coli* [4]. Swimmers respond chemotactically to several amino acids, and can adapt perfectly to external signals [17]. When grown on hard agar swimmers differentiate into highly motile, hyperflagellated, multi-nucleated, non-chemotactic swarmer cells that may be as long as 50-100 μm , and that move coordinately as “rafts” in the slime they produce [18,19]. During pattern formation on hard surfaces swarmer cells are found mainly at the leading edge of the colony, while swimmers dominate in the interior of the colony [8, 16, 18, 20]. More and more effort is put into understanding the mechanism of swarming, but to date little is known about how cells swarm and how cells undergo transitions between swimmers and swarmers [18, 19, 21–25], but understanding these processes and how they affect colonization could lead to improved treatments of the diseases *P. mirabilis* can cause.

Traditionally, formation of periodic cell-density patterns in *Proteus* colonies has been interpreted as a result of periodic changes in velocity of the colony’s front, caused by the cyclic process of differentiation and dedifferentiation of swimmers into swarmers (see [8]). Douglas and Bisset (1976) described a regime for some strains of *P. mirabilis* in which swarmers form a continuously moving front, while concentric rings of high cell density form well behind that front. This suggests that pattern formation can occur in the absence of cycles of differentiation and dedifferentiation. The similarity between this mode of pattern formation and that of *Salmonella* led us to ask whether the underlying mechanism for pattern formation in *P. mirabilis* might also be chemotactic aggregation of the actively moving swimmers behind the colony front.

A number of mathematical models of colony front movement have been proposed, and in all of them swimmer cells are nonmotile and swarming motility is described as a degenerate diffusion, in that swarmers only diffuse when their density exceeds a critical value [26–30]. The front propagation patterns as a function of various parameters in one model are given in [28]. Although these models can reproduce the colony front dynamics, it remains to justify modeling the swarming motility as a diffusion process, since it is likely that the cell-substrate interaction is important. To replicate a periodically propagating front, Ayati showed that swarmers must de-differentiate if and only if they have a certain number of nuclei [29, 30]. It was shown that this may result from diffusion limitations of intracellular chemicals, but biological evidence supporting this assumption is lacking, and further investigation is needed to understand the mechanism of front propagation.

Here we report new experimental results for a continuously-expanding front and show that after some period of growth, swimmer cells in the central part of the colony begin streaming inward and form a number of complex multicellular structures, including radial and spiral streams as well as concentric rings. These observations suggest that swimmer cells are also motile and communication between them may play a crucial role in the formation of the spatial patterns.

However, additional questions raised by the new findings include: (1) what induces the inward movement of swimmer cells, (2) why they move in streams, (3) why radial streams quickly evolve into spiral streams, and (4) quite surprisingly, why all the spirals wind counterclockwise when viewed from above. To address these questions we developed a hybrid cell-based model in which swimmer cells communicate by excreting a chemoattractant to which they also respond. The model has provided biologically-based answers to the questions above and guided new experiments. We have also developed a continuum chemotaxis model for patterning using moment closure methods and perturbation analysis [31], and we discuss how the classical models had to be modified for *Proteus* patterning.

Results

Experimental findings

Previous experimental work focused on expansion of the colony and neglected the role of swimmers in the pattern formation process. The experimental results reported here represent a first step toward understanding their role. After a drop of *P. mirabilis* culture is inoculated on a hard agar-like surface containing rich nutrient, the colony grows and expands. Under the conditions used here, the colony front expands continuously initially as a disc of uniform density (Figure 2). The swimmers exist at the periphery of the colony, and the mean length of the cells decreases towards the center, as observed by others [32]. After a period of growth, swimmer cells behind the leading edge start to stream inward, forming a number of complex patterns (Figure 1). The swimmer population first forms a radial spoke-like pattern in an annular zone on a time scale of minutes, and then cells follow these radial streams inward (1a). The radial streams soon evolve into spirals streams, with aggregates at the inner end of each arm (1b). A characteristic feature of this stage is that the spirals always wind counterclockwise when viewed from above. Different aggregates may merge, forming more complex attracting structures such as rotating rings and traveling trains (1b, c). Eventually the motion stops and these structures freeze and form the stationary elements of the pattern (1b, c). Later, this dynamic process repeats at some distance from the first element of the pattern, and sometimes cells are recruited from that element. In this way, additional elements of the permanent pattern are laid down (1c). On a microscopic level, transition to the aggregation phase can be recognized as transformation of a monolayer of cells into a complex multi-layered structure. Not every pattern is observable in repeated experiments, (for example, no observable rotating rings can be identified in (1d)), probably due to sensitivity to noise in the system and other factors that require further investigation, variations in nutrient availability, etc., but the radial and spiral streams seem to be quite reproducible.

These new findings pose challenges to the existing theories of concentric ring formation in which swimmer cells are believed to be non-motile. Additional questions arise regarding the mechanism(s) underlying the formation of radial and spiral streams, rings and trains by swimmers, and what determines the chirality of the spiral streams. The macroscopic patterns are very different and more dynamic than the patterns formed in *Escherichia coli* or *Salmonella typhimurium* colonies [1–3], where cells interact indirectly via a secreted attractant, but the fact that swimmers move up the cell density gradient is quite similar. The non-equilibrium dynamics suggests intercellular communication between individual swimmer cells. We deter-

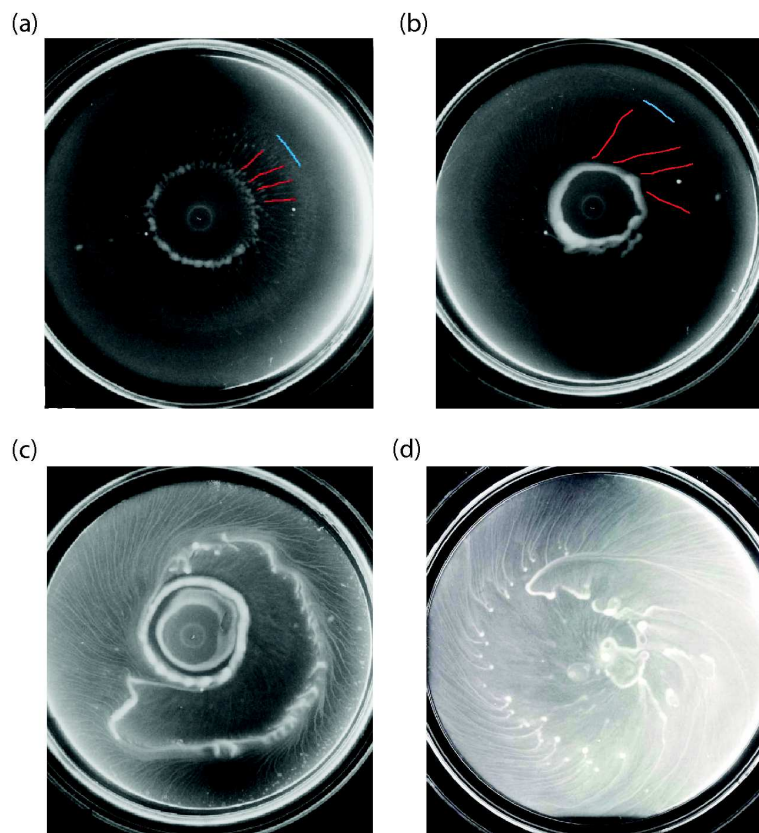


Figure 1. The evolution of a *P. mirabilis* colony. Time after inoculation: (a) 8.5 hours, (b) 9 hours, and (c) 11 hours. (a) initially homogeneous bacterial lawn breaks into radial spokes in the central region of the colony, then bacteria and bacterial aggregates stream inwards following the radial spokes. (b) the radial streams gradually transform into counterclockwise spirals, and the inner ends of each arm join together to form a solid toroidal mass. (c) a second rotating ring forms with spirals that arise further from the center, and a moving train of high cell density forms at some distance from the ring. In (a) and (b), the colony front is highlighted in blue, and a few arms of the streams are highlighted in red. In (c) the colony has covered the entire plate. (d) A different experiment that shows only stream formation without the structure of ring elements.

mined that swimmer cells extracted from these patterns are chemotactic towards several amino acids, including Aspartate, Methionine and Serine (see Table 1). In the following we provide an explanation of the radial and spiral streams using a hybrid cell-based model.

The hybrid cell-based model

The spatial patterns of interest here are formed in the center of the colony where cells are primarily swimmers, and the role of swimmers is mainly to advance the front and to affect the

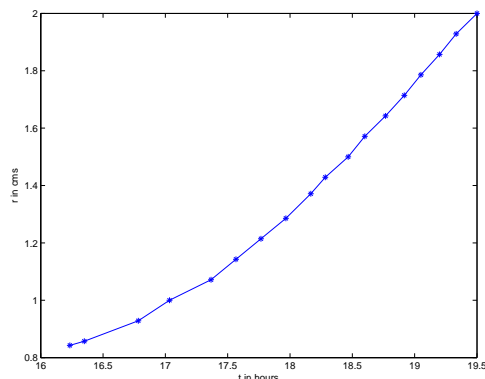


Figure 2. The radius of the colony as a function of the real time. Extracted from the supporting movie.

swimmer population by differentiation and de-differentiation. Thus we first focus on modeling the dynamics in the patterning zone in the colony center (Figure 3a), and later we incorporate the colony front as a source of swimmers (see Figure 7). This enables us to avoid unnecessary assumptions on the poorly-understood biology of swarming and the transition between the two phenotypes. As noted earlier, swimmer cells are chemotactic to certain factors in the medium, and we assume that they communicate via a chemoattractant that they secrete and to which they respond. Therefore the minimal mathematical model involves equations for the signal transduction and movement of individual cells, and for the spatio-temporal evolution of the extracellular attractant and the nutrient in the domain shown in Figure 3b. We first focus on understanding the radial and spiral stream formation, which occurs rapidly, and during which the nutrient is not depleted and cells grow exponentially. During this period the nutrient equation is uncoupled from the cell equations and can be ignored.

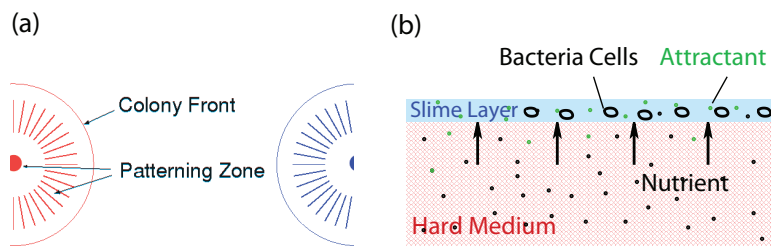


Figure 3. (a) The colony front and the patterning zone. (b) A vertical cross-section of the system. The lower layer is hard agar that contains nutrients, and the top layer is slime generated during colony expansion. Swimmers move in the layer of slime, absorb nutrients that diffuse upward, and secrete attractant. Bacterial flagella are not shown.

P. mirabilis is genetically close to *Escherichia coli*, and all the chemotaxis-related genes of *Escherichia coli* have been identified in *Proteus* [17]. *P. mirabilis* cells swim using a run-and-tumble strategy, which consists of more-or-less straight runs punctuated by random turns.

In the absence of an attractant gradient the result is an unbiased random walk, with mean run time ~ 1 s and mean tumble time ~ 0.1 s. In the presence of an attractant gradient, runs in a favorable direction are prolonged, and by ignoring the tumbling time, which is much shorter than the run time, the movement of each cell can be treated as an independent velocity jump process with a random turning kernel and a turning rate determined by intracellular variables that evolve in response to extracellular signals [33]. The signal transduction pathway for chemotaxis is complex and has been studied extensively in *Escherichia coli*, both experimentally and mathematically [34–40]. However the main processes are relatively simple, and consist of fast excitation in response to signal changes, followed by adaptation that subtracts out the background signal. Given the genetic similarity between *P. mirabilis* and *Escherichia coli*, we describe motility and signal transduction of each cell using the key ideas used successfully for *Escherichia coli* [41].

- Each swimmer cell (with index i) is treated as a point and characterized by its location \mathbf{x}^i , velocity \mathbf{v}^i , cell-cycle clock A^i and intracellular variables \mathbf{y}^i .
- Signal transduction of each cell is described by the simple model used in [33], which captures the main dynamics of the signal transduction network,

$$\frac{dy_1^i}{dt} = \frac{G(S(\mathbf{x}, t)) - (y_1^i + y_2^i)}{t_e}, \quad (1)$$

$$\frac{dy_2^i}{dt} = \frac{G(S(\mathbf{x}, t)) - y_2^i}{t_a}, \quad (2)$$

where t_e, t_a with $t_e \ll t_a$ are constants characterizing the excitation and adaptation time scales, S is the local attractant concentration and $G(S(\mathbf{x}, t))$ models detection and transduction of the signal. Here the variable y_1 is the one that excites and adapts to the signal. It has a similar role as CheY_P in the signal transduction network. The variable y_2 causes the adaptation, which models the methylation level of receptors.

- The turning rate and turning kernel are

$$\lambda^i = \lambda_0 \left(1 - \frac{y_1^i}{\eta + |y_1^i|} \right), \quad T(\mathbf{v}, \mathbf{v}') = \frac{1}{|\mathbf{V}|}, \quad (3)$$

which assumes no directional persistence [42].

- Since the slime layer is very thin, typically $\sim 10\mu\text{m}$, we restrict cell movement to two dimensions.
- Each cell divides every 2 h and is replaced by two identical daughter cells of age $A = 0$.

We assume that cells secrete attractant at a constant rate γ and that it is degraded by a first-order process. The resulting evolution equation for the attractant is

$$\frac{\partial S}{\partial t} = D_s \Delta S + \gamma \sum_{n=1}^N \delta(\mathbf{x} - \mathbf{x}^i) - \mu S \quad (4)$$

For simplicity, we also restrict reaction and diffusion of the attractant to two space dimensions, which is justified as follows. Since no attractant is added to the substrate initially, which is much thicker than the slime layer, we assume that the attractant level is always zero in the substrate. We further assume that the flux of the attractant at the interface of the two layers is linear in the difference of its concentration between the two layers. Thus the loss of attractant due to diffusion to the agar can be modeled as a linear degradation, and the degradation constant μ in (4) reflects the natural degradation rate and the flux to the substrate.

In the numerical investigations described below, (4) is solved on a square domain using the ADI method with no-flux boundary conditions, while cells move off-grid. For each time step Δt (\ll mean run time), (1), (2) are integrated for each cell and the velocity and position are updated by Monte Carlo simulation. Transfer of variables to and from the grid is done using bilinear interpolating operators. A detailed description of the numerical scheme is given in Appendix A of [31].

Radial streams result from an instability of the uniform cell distribution

Radial streams appear after several hours of bacterial growth, and before their emergence, the cell density is uniform in the colony, except at the inoculation site. At this stage the attractant concentration can be approximated by a cone-like profile centered at that site. Here we show that starting from this initial condition, the mechanism introduced above can explain radial stream formation. In the numerical investigations below we assume that $t_e = 0$ and $G(S) = S$ for simplicity. Therefore,

$$\begin{aligned} \frac{dy_2^i}{dt} &= \frac{S(\mathbf{x}, t) - y_2^i}{t_a}, \\ y_1^i &= S(\mathbf{x}, t) - y_2^i. \end{aligned}$$

We specify an initial attractant gradient of $4 \times 10^{-3} \mu\text{M}/\text{cm}$ in a disk of radius 1.5 cm, centered at the center of the domain, with zero attractant at the boundary of the disk. For compatibility with later computations on a growing disk, we initially distribute 10^4 cells/cm² randomly within the disk. (If cells are initially distributed throughout the square domain cells near the four corners, outside the influence of the initial gradient, aggregate into spots, as is observed in *Escherichia coli* as well [31].) Figure 4 shows how this distribution evolves into radial streams that terminate in a high-density region at the center, as expected. One can understand the breakup into streams as follows.

Whether or not there is a macroscopic attractant gradient, cells bias their run lengths in response to the local concentration and the changes they measure via the perceived Lagrangian derivative of attractant along their trajectory. In this situation, the small local variations in cell density produce local variations in attractant to which the cells respond. In the absence of a macroscopic gradient, an initially-uniform cell density evolves into a high cell density network, which in turn breaks into aggregates, and then nearby aggregates may merge ([31], Figure 4.4), as is also observed experimentally in *E. coli* ([1]. If we describe the cell motion by a 1-D velocity jump process, a linear stability analysis of the corresponding continuum equations predicts that the uniform distribution is unstable, and breaks up into a well-defined spatial pattern ([31]), Figure 4.2, 4.3). Numerical solutions of the nonlinear equations confirm this, and experiments

in which the grid size is varied show that the results are independent of the grid, given that it is fine enough [31].

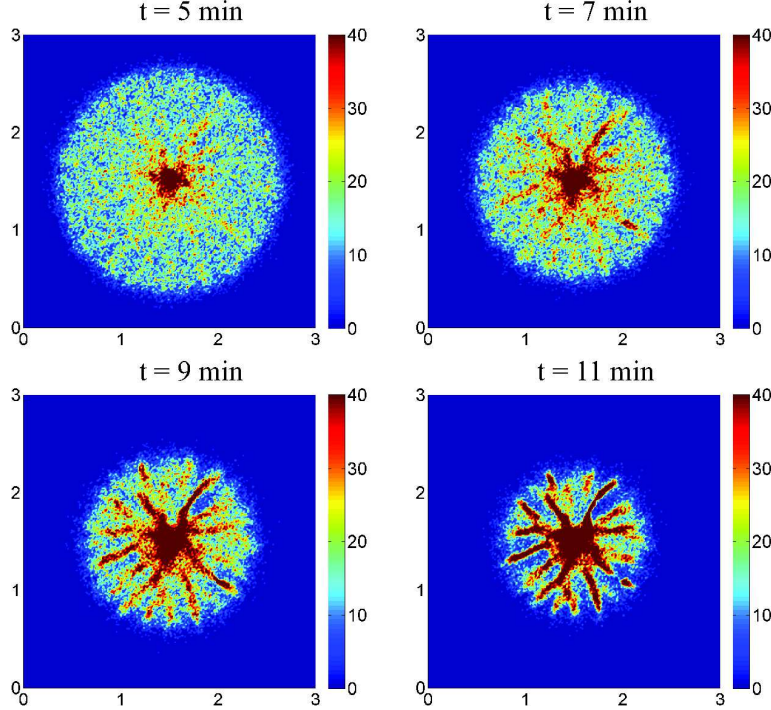


Figure 4. Simulated radial streams. The cell density profile is in units of $10^3/\text{cm}^2$. Parameters used: $\bar{s} = 20\mu\text{m/s}$, $\lambda_0 = 1/\text{s}$, $D_c = 9 \times 10^{-6}\text{cm}^2/\text{s}$, $\mu = 10^{-3}/\text{s}$, $L = 3\text{cm}$, $t_a = 5\text{s}$, $\eta = 5 \times 10^{-5}$, and the secretion rate of the attractant is $6 \times 10^{-17}\text{mol/s}$ per cell.

In the presence of a macroscopic gradient a similar analysis, taken along a 1D circular cross-section of the 2D aggregation field, predicts the breakup of the uniform distribution, but in this situation the 2D pattern of local aggregations is aligned in the direction of the macroscopic gradient. This is demonstrated in a numerical experiment in which cells are placed on a cylindrical surface with constant attractant gradient. Thus the experimentally-observed radial streams shown in Figure 1 and the theoretically-predicted ones shown in Figure 4 can be understood as the result of (i) a linear instability of the uniform cell density, and (ii) the nonlinear evolution of the growing mode, with growth oriented by the initial macroscopic gradient of attractant.

Spiral streams result from a surface-induced swimming bias

In most experiments the radial streams that arise initially rapidly evolve into spiral streams, and importantly, these spirals always wind counter-clockwise when viewed from above. The invariance of the chirality of these spirals indicates that there are other forces that act either on individual cells or on the fluid in the slime layer, and that initial conditions play no significant role. One possible explanation, which we show later can account for the observed chirality,

stems from observations of the swimming behavior of *Escherichia coli* in bulk solution and near surfaces. When far from the boundary of a container, *Escherichia coli* executes the standard run and tumble sequence, with more or less straight runs interrupted by a tumbling phase in which a new, essentially random direction is chosen. (There is a slight tendency to continue in the previous direction). However, observations of cell tracks near a surface show that cells exhibit a persistent tendency to swim clockwise when viewed from above [43–45].

Since the cells are small, the Reynolds number based on the cell length is very small ($\mathcal{O}(10^{-5})$), and thus inertial effects are negligible, and the motion of a cell is both force- and torque-free. Since the flagellar bundle rotates counter-clockwise during a run, when viewed from behind, the cell body must rotate clockwise. When a cell is swimming near a surface, the part of the cell body closer to the surface experiences a greater drag force due to the interaction of the boundary layer surrounding the cell with that at the immobile substrate surface. Suppose that the Cartesian frame has the x and y axes in the substrate plane and that z measures distance into the fluid. When a cell runs parallel to the surface in the y direction and the cell body rotates CW, the cell body experiences a net force in the x direction due to the asymmetry in the drag force. Since the flagellar bundle rotates CCW, a net force with the opposite direction acts on the flagella, and these two forces form a couple that produces the swimming bias of the cell. (Since the entire cell is also torque-free, there is a counteracting viscous couple that opposes the rotation, and there is no angular acceleration.) The closer the cell is to the surface, the smaller is the radius of curvature and the slower the cell speed. Because of the bias, cells that are once near the surface tend to remain near the surface, which increases the possibility of attachment. (In the case of *Proteus* this may facilitate the swimmer-to-swarm transition, but this is not established.) Resistive force theory has been used to derive quantitative approximations for the radius of curvature as a function of the distance of the cell from the surface and other cell-level dimensions, treating the cell body as a sphere and the flagellar bundle as a single rigid helix [45]. Cell speed has been shown to first increase and then decrease with increasing viscosity of linear-polymer solutions when cells are far from a surface [46], but how viscosity changes the bias close to a surface is not known.

The question we investigate here is whether the microscopic swimming bias of single bacteria can produce the macroscopic spiral stream formation with the correct chirality. We cannot apply the above theory rigorously, since that would involve solving the Stokes problem for each cell, using variable heights from the surface. Instead, we introduce a constant bias of each cell during the runs, *i.e.*,

$$\frac{d\mathbf{v}^i}{dt} = \varepsilon_b \frac{\mathbf{v}_i}{|\mathbf{v}_i|} \times \mathbf{k}$$

where \mathbf{k} is the normal vector to the surface, and $\varepsilon_b > 0$ measures the magnitude of the bias in the direction of swimming.

Figure 5 shows the evolution of the cell density using a bias of $\varepsilon = 0.04\pi$, which is chosen so that a cell traverses a complete circle in 50 secs, but the results are insensitive to this choice. The simulations show that the initially-uniform cell density evolves into spiral streams after a few minutes and by 12 minutes the majority of the cells have joined one of the spiral arms. The spiral streams persist for some time and eventually break into necklaces of aggregates which actively move towards the center of the domain.

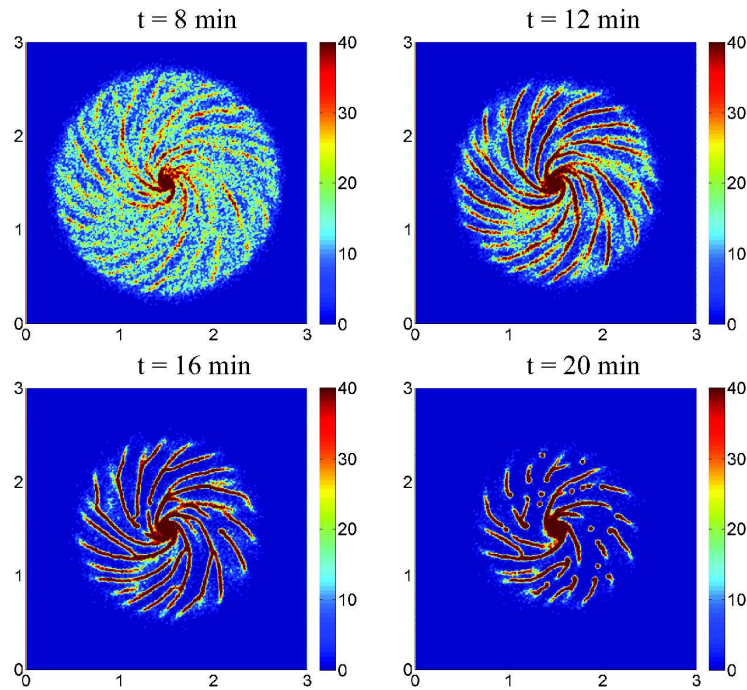


Figure 5. Simulated spiral streams in a disk using a swimming bias of $\varepsilon_b = 0.04\pi$. The initial attractant gradient is $4 \times 10^{-3} \mu\text{M}/\text{cm}$, centered as before, and all other parameters are as used for the results in Figure 4.

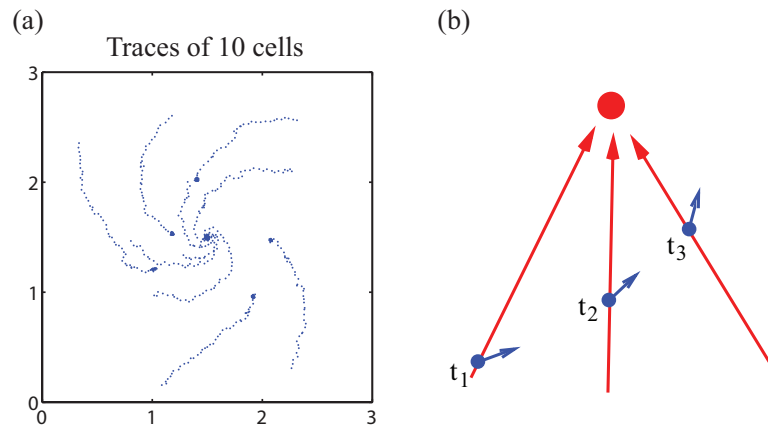


Figure 6. (a) The positions of 10 randomly chosen cells, each position recorded every 30 sec by a blue dot. (b) schematics of cell movement.

Figure 6a illustrates the positions of 10 randomly chosen cells every 30 seconds, and Figure 6b illustrates how to understand the macroscopic chirality based on the swimming bias of individual

cells. At $t = t_1$ the blue cell detects a signal gradient (red arrow) roughly in the 1 o'clock direction, and on average it swims up the gradient longer than down the gradient. Because of the clockwise swimming bias, the average drift is in the direction of the blue arrow. At $t = t_2$ it arrives at the place and 'realizes' that the signal gradient is roughly in the 12 o'clock direction, and a similar argument leads to the average net velocity at that spot. As a result of these competing influences, the cell gradually make its way to the source of attractant (the red dot) in a counterclockwise fashion. Certainly the pitch of the spirals is related to the swimming bias, but we have not determined the precise relationship. The spiral movement has also been explained mathematically in [31], where the macroscopic chemotaxis equation is derived from the hybrid model in the presence of an external force, under the shallow-signal-gradient assumption. When the swimming bias is constant, the analysis shows that this bias leads to an additional taxis-like flux orthogonal to the signal gradient.

According to the foregoing explanation, one expects spirals in the opposite direction when experiments are performed with the petri plate upside-down and patterns are viewed from the top, since in this case the relative position of the matrix and slime is inverted and cells are swimming under the surface. This prediction has been confirmed experimentally, and the conclusion is that the interaction between the cell and the liquid-gel surface is the crucial factor that determines the genesis and structure of the spirals.

Pattern formation on a growing disk

From the foregoing simulations we conclude that when the swimming bias is incorporated, the hybrid model correctly predicts the emergence of streams and their evolution into spirals of the correct chirality for experimentally-reasonable initial cell densities and attractant concentration. Next we take one more step toward a complete model by incorporating growth of the patterning domain. As we indicated earlier, the biology of swimmer/swarmer differentiation and the biophysics of movement at the leading edge are poorly understood. Consequently, we here regard the advancing front as a source of swimmer cells and prescribe a constant expansion rate as observed in experiments (Figure 2). The results of one computational experiment are shown in Figure 7, in which the colony expands outward at a speed of 0.5cm/h (as in Figure 2 after the initial lag phase), and the cells added in this process are swimmer cells. One sees that the early dynamics when the disk is small are similar to the results in Figure 5 on a fixed disk, but as the disk continues to grow the inner structure develops into numerous isolated islands, while the structure near the boundary exhibits the spirals. The juxtaposition in Figure 8 of the numerical simulation of the pattern at 5 hours and the experimental results shown in Figure 1 shows surprisingly good agreement, despite the simplicity of the model. This suggests that the essential mechanisms in the pattern formation have been identified, but others are certainly involved, since the experimental results show additional structure in the center of the disk that the current model does not replicate.

Discussion

New experimental results reported here show that swimmer cells in the center of the colony stream inward toward the inoculation site, and form a number of complex patterns, including

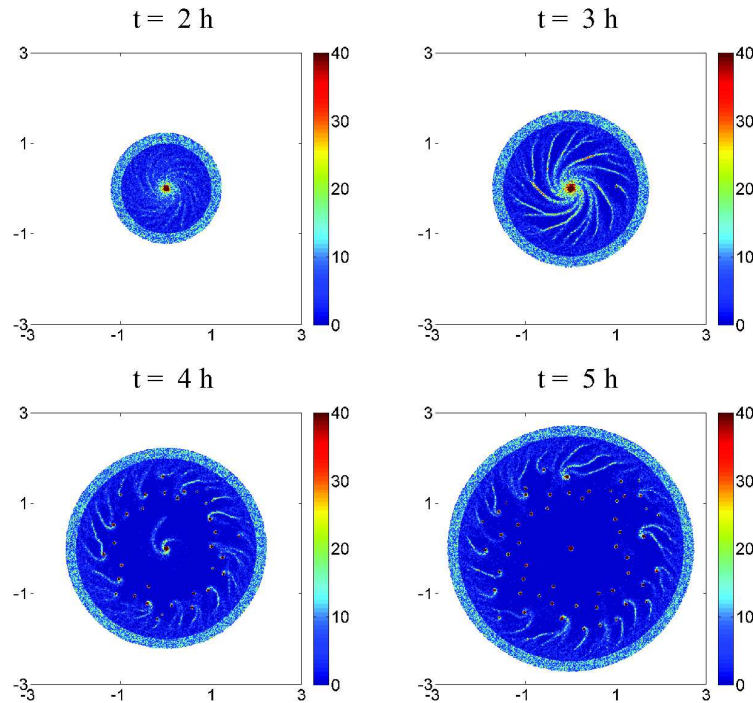


Figure 7. Streams in a growing colony. $\rho_0 = 10^4 \text{ cells/cm}^2$, $\varepsilon_b = 0.04\pi$, Other parameters used are the same as in Figure 4.

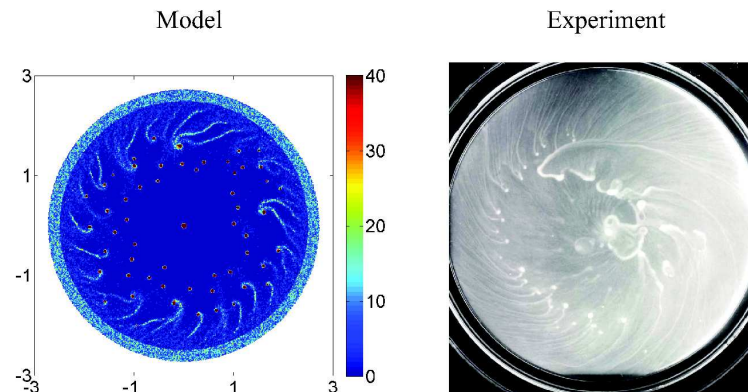


Figure 8. A comparison of predicted and observed spatial patterns. Parameters used are the same as in Figure 4.

radial and spiral streams in an early stage, and rings and traveling trains in later stages. These experiments suggest that intercellular communication is involved in the spatial pattern formation. The experiments raise many questions, including what induces the inward movement of swimmer cells, why they move in streams, why radial streams quickly evolve into spiral streams,

and finally, why all the spirals wind counterclockwise. To address these we developed a hybrid cell-based model in which we describe the chemotactic movement of each cell individually by an independent velocity jump process. We couple this cell-based model of chemotactic movement with reaction-diffusion equations for the nutrient and attractant. To numerically solve the governing equations, a Monte Carlo method is used to simulate the velocity jump process of each cell, and an ADI method is used to solve the reaction-diffusion equations for the extracellular chemicals. The hybrid cell-based model has yielded biologically-based answers to the questions raised above. Starting with an estimate of the attractant level before the onset of the radial streaming as the initial value, we predicted the formation of radial streams as a result of the modulation of the local attractant concentration by the cells. It is observed in *Escherichia coli* that 'runs' of single cells curve to the right when cells swim near a surface, and we incorporated this swimming bias by adding a constant angular velocity during runs of each cell. This leads to spiral streams with the same chirality as is observed experimentally. Finally, by incorporating growth of the patterning domain we were able to capture some of the salient features of the global patterns observed.

The streams and spirals reported here share similarities with those formed in *Dictyostelium discoideum*, where cells migrate towards a pacemaker, but there are significant differences. Firstly, the mechanism leading to aggregation is similar, in that in both cases the cells react chemotactically and secrete the attractant. However, since bacteria are small, they do a 'bakery search' in deciding how to move – detecting the signal while moving, and constantly modulating their run time in response to changes in the signal. In contrast, *D. discoideum* is large enough that it can measure gradients across its length and orient and move accordingly. Thus bacteria measure temporal gradients whereas amoeboid cells such as *D. discoideum* measure spatial gradients. In either case the cells respond locally by forming streams and migrate up the gradient of an attractant. However, spirals are less ubiquitous in *D. discoideum*, and when they form they can be of either handedness, whereas in *P. mirabilis*, only spirals wound counterclockwise when viewed from above have been observed, which emphasizes the importance of the influence of the cell-substrate interaction when cells swim close to the surface. Experiments in which the patterning occurs in an inverted petri dish lead to spirals with an opposite handedness when viewed from above, which further support our explanation. Our results imply that the spatial patterns observed in *P. mirabilis* can be explained by the chemotactic behavior of swimmer cells, and suggest that differentiation and de-differentiation of the cells at the leading edge does not play a critical role in patterning, but rather serves to expand the colony under appropriate conditions. A future objective is to incorporate a better description of the dynamics at the leading edge when more biological information is available.

The spatial patterns reported here are also different from those observed in other bacteria such as *Escherichia coli* or *Bacillus subtilis*. In the latter, fractal and spiral growth patterns have been observed [5,6], and these patterns form primarily at the leading edge of the growing colony. There cell motility plays a lesser role and the limited diffusion of nutrient plays an important role in the pattern formation.

Of course the experimental reality is more complicated than that which our model describes. For instance, the nutrient composition is very complex and nutrient depletion may occur at a later stages such as during train formation. Further, cells may become non-motile for various reasons, and these factors may play a role in the stabilization of the ring patterns. Another

important issue is the hydrodynamic interaction of the swimmer cells with fluid in the slime layer. When cell density is low and cells are well separated we can approximate their movement by independent velocity jump processes plus a swimming bias, but when the cell density is high the cell movement is correlated through the hydrodynamic interactions and this must be taken into account. This hydrodynamic interaction may be an important factor in the formation of the trains observed in experiments.

The individual cell behavior, including the swimming bias, has been embedded in a continuum chemotaxis equation derived by analyzing the diffusion limit of a transport equation based on the velocity jump process [31]. The resulting equation is based on the assumption that the signal gradient is shallow and the predicted macroscopic velocity in this regime is linear in the signal gradient. A novel feature of the result is that the swimming bias at the individual cell level gives rise to an additional taxis term orthogonal to the signal gradient in this equation. However in the simulations of the patterns presented here we observe steep signal gradients near the core of the patterns and within the streams, and therefore in these regimes the assumptions underlying the continuum chemotaxis model are not valid. A statistical analysis of cell trajectories in the results from the cell-based model reveals saturation in the macroscopic velocity and a decreasing diffusion constant as the signal gradient grows, which suggests that in the limiting case of large gradients, the macroscopic equation for cell density will simply be a transport equation with velocity depending on the signal gradient.

Materials and Methods

Chemotaxis analysis of swimmer cells

Positive chemotaxis toward each of the common 20 amino acids was tested using the drop assay. Each amino acid was tested at the following concentrations: .1M, 10mM , 1mM, 10 μ M, and 1 μ M.

Chemotaxis on semi-solid agar

Chemotaxis of swimmer cells towards single amino acids was tested using 0.3% agar plates with different thickness of substrate layer(10 and 20 ml). Each amino acid was used in concentrations varying from 0.25mM to 7.5mM in both thicknesses of agar. The plates were point inoculated and placed in a humid chamber at room temperature for at least 20 hrs. Bacteria growing on 10 and 20 ml plates with 0.001M of Aspartate, Methionine and Serine formed dense moving outer ring which we interpret as a chemotactic ring. Bacteria grown on all remaining amino acids produced colonies with the higher density at the point of inoculation and homogeneous cell distribution in the rest of the colony.

Numerical algorithm

In the implementation of the cell-based model, cell motion is simulated by a standard Monte Carlo method in the whole domain, while the equations for extracellular chemicals are solved by an alternating direction method on a set of rectangular grid points . In this appendix, we present

the numerical algorithm in a two-dimensional domain with only one chemical – the attractant – involved. Each cell is described by its position (x_1^i, x_2^i) , internal variables (y_1^i, y_2^i) , direction of movement θ^i and age T^i (the superscript i is the index of the cell). Concentration of the attractant is described by a discrete function defined on the grid for the finite difference method (Figure 9, left). We denote the time step by k , the space steps by h_1 and h_2 .

Since two components of the model live in different spaces, two interpolating operators are needed in the algorithm. \mathcal{T}_{gc} is used to evaluate the attractant concentration that a cell senses. For a cell at (x_1^i, x_2^i) , inside the square with vertex indices $(n-1, m-1)$, $(n, m-1)$, $(n-1, m)$ and (n, m) , $\mathcal{T}_{gc}(x_1^i, x_2^i)$ is defined by the bi-linear function:

$$\mathcal{T}_{gc}(x_1^i, x_2^i) = \frac{A_4}{A} S_{n-1, m-1} + \frac{A_3}{A} S_{n, m-1} + \frac{A_2}{A} S_{n-1, m} + \frac{A_1}{A} S_{n, m} \quad (5)$$

	.1M	10mM	1mM	10 μm	1 μm
Ala	+	+	-	-	-
Arg	-	-	-	-	-
Asn	-	+	-	-	-
Asp	+	-	+	+	+
Cys	-	-	+	+	-
Glu	+	+	-	-	-
Gln	-	-	-	-	-
Gly	+	+	-	-	-
His	+	+	-	-	-
Ile	-	-	-	-	-
Leu	-	-	-	-	-
Lys	-	-	-	-	-
Met	+	+	-	-	-
Phe	-	+	+	-	-
Pro	-	-	-	-	-
Ser	+	+	+	+	-
Thr	+	-	-	-	-
Trp	-	-	-	-	-
Val	-	-	-	-	-

Table 1. Amino acid drop assay. *Proteus* cells were collected from the inner area of a growing colony, approximately 1 hr before a projected onset of a streaming phase. Microscopic examination revealed that 90% of cells were 1 to 2 cell length. Cells were resuspended in a minimal growth medium to the OD=.1 to .15 (similar results were obtained with the cells grown in a liquid culture) Drop Assay. 500 μL minimal growth medium, 200 μL of cell culture (OD=.1 to .15), and 240 μL of 1% Methyl cellulose were combined in a 10x35 mm culture dish and mixed until a homogenous state. 4 μL of a respective amino acid solution was added to the center. Cell density distribution in the dish was analyzed after 20-25 minutes. Addition of H_2O was used as a control. Increase in the cell density in the center indicates that a respective amino acid is an attractant.

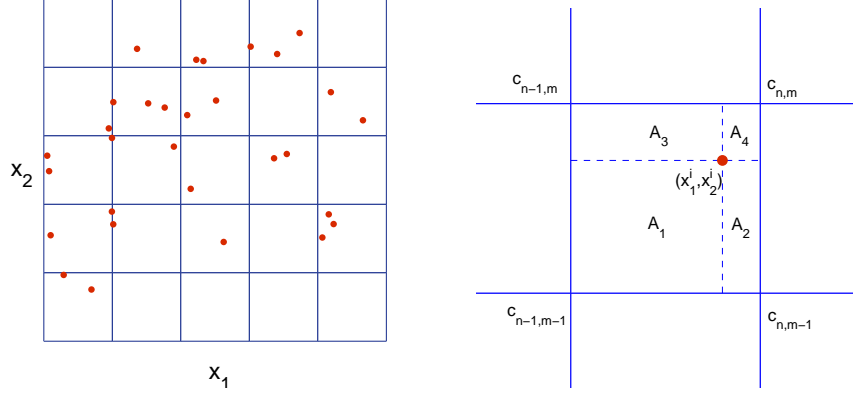


Figure 9. Numerical algorithm. Left: a schematic figure of the domains. The reaction-diffusion equations are solved on the grid, while the cells can move around the whole domain. Right: the area fractions used in defining the interpolators (5, 6).

where $A = h_1 h_2$ and $A_j, j = 1, 2, 3, 4$ are the area fractions (Figure 9, right). On the other hand, the attractant secreted by cells is interpolated as increments at the grid points by \mathcal{T}_{cg} . Suppose during one time step k , a cell staying at (x_1^i, x_2^i) secretes Δ amount of attractant, we then interpolate the increment of the attractant concentration at the neighboring grid points as follows:

$$\mathcal{T}_{cg}(\mathbf{x}^i; p, q) = \begin{cases} \frac{A_4 \Delta}{A^2}, & (p, q) = (n-1, m-1); \\ \frac{A_3 \Delta}{A^2}, & (p, q) = (n, m-1); \\ \frac{A_2 \Delta}{A^2}, & (p, q) = (n-1, m); \\ \frac{A_1 \Delta}{A^2}, & (p, q) = (n, m); \\ 0, & \text{otherwise.} \end{cases} \quad (6)$$

We consider here a periodic boundary condition. The detailed computing procedure is summarized as follows.

S1 Initialization.

- (a) Initialize the chemical fields.
- (b) Initialize the list of swimmer cells. Each cell is put in the domain with random position, moving direction and age. \mathbf{y}^i is set to be 0.

S2 For time step l ($= 1$ initially), update the data of each cell.

- (a) Determine the direction of movement θ^i by the turning kernel.
 - i) Generate a random number $r \in U[0, 1]$;
 - ii) If $r < 1 - e^{-\lambda^i k}$, update θ^i with a new random direction.
- (b) $(x_1^i, x_2^i)_l \leftarrow (x_1^i, x_2^i)_{l-1} + (sk \cos \theta^i, sk \sin \theta^i)$. Apply periodic boundary condition to make sure (x_1^i, x_2^i) inside the domain,

- (c) $(T^i)_l \leftarrow (T^i)_{l-1} + k$. If $(T^i)_l \geq 2$ hours, then divide the cell into two daughter cells. This step is only considered when cell growth is considered.
- (d) Update (y_1^i, y_2^i) by the equations for the internal dynamics.
- i) Determine the attractant concentration before the cell moves $(S^i)_{l-1}$ and after the cell moves $(S^i)_l$ by using the interpolating operator \mathcal{T}_{gc} .
 - ii) Estimate the attractant level during the movement by $S^i(t) = (S^i)_{l-1} \frac{t-lk}{k} + (S^i)_l \frac{lk+k-t}{k}$ and integrate equation for y_2^i to get $(y_2^i)_l$.
 - iii) $(y_1^i)_l \leftarrow G(S) - (y_2^i)_l$.

S3 Compute the source term of the attractant $f^{l-\frac{1}{2}}$ due to the secretion by the cells using the interpolator \mathcal{T}_{cg}

$$f_{p,q}^{l-\frac{1}{2}} = \sum_i (\mathcal{T}_{cg}((\mathbf{x}^i)_{l-\frac{1}{2}}; p, q)),$$

where $\Delta = \gamma k$.

S4 Apply the alternating direction implicit method to the equation of the attractant:

$$\begin{aligned} \frac{S_{p,q}^{l-1/2} - S_{p,q}^{l-1}}{k/2} &= D_s \frac{S_{p+1,q}^{l-1/2} - 2S_{p,q}^{l-1/2} + S_{p-1,q}^{l-1/2}}{h_x^2} \\ &\quad + D_s \frac{S_{p,q+1}^{l-1} - 2S_{p,q}^{l-1} + S_{p,q-1}^{l-1}}{h_x^2} - \gamma \frac{S_{p,q}^{l-1} + S_{p,q}^{l-1/2}}{2} + f_{p,q}^{l-\frac{1}{2}}, \\ \frac{S_{p,q}^l - S_{p,q}^{l-1/2}}{k/2} &= D_s \frac{S_{p+1,q}^{l-1/2} - 2S_{p,q}^{l-1/2} + S_{p-1,q}^{l-1/2}}{h_x^2} \\ &\quad + D_s \frac{S_{p,q+1}^l - 2S_{p,q}^l + S_{p,q-1}^l}{h_x^2} - \gamma \frac{S_{p,q}^{l-1/2} + S_{p,q}^l}{2} + f_{p,q}^{l-\frac{1}{2}}. \end{aligned}$$

For the boundary grid points, use the periodic scheme.

S5 $l \leftarrow l + 1$. If $lk \leq T_0$, repeat **S2-S4**; otherwise, return.

Acknowledgments

CX is supported by the Mathematical Biosciences Institute under the US NSF Award 0635561. HGO is supported by NIH grant GM 29123, NSF Grant DMS 0817529 and the University of Minnesota Supercomputing Institute.

References

1. E. O. Budrene and H. C. Berg. Complex patterns formed by motile cells of *escherichia coli*. *Nature*, 349(6310):630–633, February 1991.
2. E. O. Budrene and H. C. Berg. Dynamics of formation of symmetrical patterns by chemotactic bacteria. *Nature*, 376(6535):49–53, 1995.

3. D. Woodward, R. Tyson, M. Myerscough, J. Murray, E. Budrene, and H. Berg. Spatio-temporal patterns generated by *Salmonella typhimurium*. *Biophysical Journal*, 68:2181–2189, 1995.
4. H. C. Berg. Symmetries in bacterial motility. *Proc. Natl. Acad. Sci. (USA)*, 93(25):14225–8, 1996.
5. E. Ben-Jacob, O. Schochet, A. Tenenbaum, I. Cohen, and A. Czirok. Generic modelling of cooperative growth patterns in bacterial colonies. *Nature*, 368(6466):46, March 1994.
6. E. Ben-Jacob, I. Cohen, A. Czirok, T. Vicsek, and D. L. Gutnick. Chemomodulation of cellular movement, collective formation of vortices by swarming bacteria, and colonial development. 238(1):181–, 1997.
7. K. Bisset and C. Douglas. A continuous study of morphological phase in the swarm of proteus. *J. Med. Microbiol.*, 9:229–31, 1976.
8. O. Rauprich, M. Matsushita, C. Weijer, F. Siegert, S. Esipov, and J. Shapiro. Periodic phenomena in *Proteus mirabilis* swarm colony development. *J. Bacteriol*, 178(22):6525–6538, 1996.
9. Avraham Be’er, H. P. Zhang, E-L. Florin, Shelley M Payne, Eshel Ben-Jacob, and Harry L Swinney. Deadly competition between sibling bacterial colonies. *Proc Natl Acad Sci U S A*, 106(2):428–433, Jan 2009.
10. Yilin Wu, A. Dale Kaiser, Yi Jiang, and Mark S Alber. Periodic reversal of direction allows myxobacteria to swarm. *Proc Natl Acad Sci U S A*, 106:1222–1227, 2009.
11. J. A. Shapiro. Thinking about bacterial populations as multicellular organisms. *Ann Rev Microbiol*, 52:81–104, 1998.
12. P. Zunino, C. Piccini, and C. Fajardo. Flagellate and non-flagellate proteus mirabilis in the development of experimental urinary tract infection. *Microb. Pathog.*, 16(5):379–85, 1994.
13. H. Mobley and R. Belas. Swarming and pathogenicity of proteus mirabilis in the urinary tract. *Trends Microbiol.*, 3(7):280–284, 1995.
14. A. Jansen, C. Lockett, D. Johnson, and H. Mobley. Visualization of proteus mirabilis morphotypes in the urinary tract: the elongated swarmer cell is rarely observed in ascending urinary tract infection. *Infct. Immun.*, 71(6):3607–13, 2003.
15. B. Jones, E. Mahenthiralingam, N. Sabbuba, and D. Stickler. Role of swarming in the formation of crystalline proteus mirabilis biofilms on urinary catheters. *J. Med. Microbiol.*, 54(9):807–813, 2005.
16. G. Hauser. *Über Faulnissbakterien und deren Beziehungen zur Septicämie*. F. C. W. Vogel, Leipzig, Germany., 1885.

17. Melanie M Pearson, Mohammed Sebahia, Carol Churcher, Michael A Quail, Aswin S Seshasayee, Nicholas M Luscombe, Zahra Abdellah, Claire Arrosmith, Becky Atkin, Tracey Chillingworth, Heidi Hauser, Kay Jagels, Sharon Moule, Karen Mungall, Halina Norbertczak, Ester Rabbino-witsch, Danielle Walker, Sally Whithead, Nicholas R Thomson, Philip N Rather, Julian Parkhill, and Harry L T Mobley. Complete genome sequence of uropathogenic proteus mirabilis, a master of both adherence and motility. *J Bacteriol*, 190(11):4027–4037, 2008.
18. F. D. Williams. Nature of the swarming phenomenon in *Proteus*. *Ann. Rev. Microbiol.*, 32:101–22, 1978.
19. G. Fraser and C. Hughes. Swarming motility. *Curr. Opin. in Microbiol.*, 2(0):630–635, 1999.
20. C. Douglas and K. Bisset. Development of concentric zones in the *Proteus* swarm colony. *J. Med. Microbiol.*, 9:497–500, 1976.
21. P. Rather. Swarmer cell differentiation in *Proteus mirabilis*. *Environmental Microbiology*, 7(8):1065–1073, 2005.
22. Julien Tremblay, Anne-Pascale Richardson, Francois Lepine, and Eric Deziel. Self-produced extracellular stimuli modulate the pseudomonas aeruginosa swarming motility behaviour. *Environ Microbiol*, 9(10):2622–2630, 2007.
23. Daniel B Kearns. A field guide to bacterial swarming motility. *Nat Rev Microbiol*, 8(9):634–644, 2010.
24. H. P. Zhang, Avraham Be’er, E-L. Florin, and Harry L Swinney. Collective motion and density fluctuations in bacterial colonies. *Proc Natl Acad Sci U S A*, 107(31):13626–13630, Aug 2010.
25. Yilin Wu, Basarab G Hosu, and Howard C Berg. Microbubbles reveal chiral fluid flows in bacterial swarms. *Proc Natl Acad Sci U S A*, 108(10):4147–4151, Mar 2011.
26. S. Esipov and J. Shapiro. Kinetic model of *Proteus Mirabilis* swarm colony development. *J. Math. Biol.*, 36:249–268, 1998.
27. G. Medvedev, T. Kaper, and N. Kopell. A reaction-diffusion system with periodic front dynamics. *SIAM J. App. Math.*, 60(5):1601–1638, 2000.
28. A. Czirók, M. Matsushita, and T. Vicsek. Theory of periodic swarming of bacteria: application to proteus mirabilis. *Phys Rev E*, 63, 2001.
29. Bruce P Ayati. A structured-population model of proteus mirabilis swarm-colony development. *J Math Biol*, 52(1):93–114, 2006.
30. B. Ayati. Modeling the role of the cell cycle in regulating *proteus mirabilis* swarm-colony development. *Applied Mathematics Letters*, 20(8):913–918, 2007.

31. C. Xue and H. G. Othmer. Multiscale models of taxis-driven patterning in bacterial populations. *SIAM J. Appl. Math.*, 70(1):133–167, 2009.
32. T. Matsuyama, Y. Takagi, Y. Nakagawa, H. Itoh, J. Wakita, and M. Matsushita. Dynamic aspects of the structured cell population in a swarming colony of proteus mirabilis. *J. Bacteriol.*, 182(2):385–393, 2000.
33. R. Erban and H. G. Othmer. From individual to collective behavior in bacterial chemotaxis. *SIAM J. Appl. Math.*, 65(2):361–391, 2004.
34. R. Lux and W. Shi. Chemotaxis-guided movements in bacteria. *Crit. Rev. Oral. Biol. Med.*, 15(4):207–20, 2004.
35. G. Wadhams and J. Armitage. Making sense of it all: bacterial chemotaxis. *Nat. Rev. Mol. Cell Biol.*, 5(12):1024–37, 2004.
36. R. Bourret, Borkovich K, and M. Simon. Signal transduction pathways involving protein phosphorylation in prokaryotes. *Annu. Rev. Biochemistry*, 60:401–441, 1991.
37. Peter A. Spiro, John S. Parkinson, and Hans G. Othmer. A model of excitation and adaptation in bacterial chemotaxis. *Proc. Nat. Acad. Sci.*, 94(14):7263–7268, 1997.
38. T. S. Shimizu, S. V. Aksenov, and D. Bray. A spatially extended stochastic model of the bacterial chemotaxis signalling pathway. *J. Mol. Biol.*, 329:291–309, 2003.
39. B. A. Mello and Y. Tu. Quantitative modeling of sensitivity in bacterial chemotaxis: the role of coupling among different chemoreceptor species. *PNAS*, 100:8223–8228, 2003.
40. C. V. Rao, J. R. Kirby, and A. P. Arkin. Design and diversity in bacterial chemotaxis: A comparative study in *Escherichia coli* and bacillus subtilis. *PLoS Biol*, 2(2):E49, 2004.
41. Radek Erban. *From individual to collective behavior in biological systems*. PhD thesis, University of Minnesota, 2005.
42. H. G. Othmer, S. R. Dunbar, and W. Alt. Models of dispersal in biological systems. *J. Math. Biol.*, 26(3):263–298, 1988.
43. P. D. Frymier, R. M. Ford, H. C. Berg, and P. T. Cummings. Three-dimensional tracking of motile bacteria near a solid planar surface. *PNAS*, 92:6195–6199, 1995.
44. W. R. DiLuzio, L. Turner, M. Mayer, P. Garstecki, D. B. Weibel, H. C. Berg, and G. M. Whitesides. *Escherichia coli* swim on the right-hand side. *Nature*, 435(7046):1271–4, June 30 2005.
45. E. Lauga, W. R. DiLuzio, G. M. Whitesides, and H. A. Stone. Swimming in circles: Motion of bacteria near solid boundaries. *Biophys. J.*, 90:400–412, 2006.
46. Yukio Magariyama and Seishi Kudo. A mathematical explanation of an increase in bacterial swimming speed with viscosity in linear-polymer solutions. *Biophys J*, 83(2):733–739, Aug 2002.